STUDY ON FACTORS AFFECTING ICE SPIKE FORMATION IN WATER-BASED PHASE CHANGE ENERGY STORAGE DEVICE

Ziquan Yan[a], You Wang[a], Ziliang Zhu[a], Hanbing Ke[b], Mei Lin[a], Yining Wu[a*], Qiuwang Wang[a]

[*a]School of Energy and Power Engineering, Xi'an Jiaotong University, Xi'an, China

[b]Science and Technology on Thermal Energy and Power Laboratory, Wuhan, 430205, Hubei, China

[*]Corresponding author; E-mail: ynwu @mail.xjtu.edu.cn

During the water-ice phase transition process in energy storage devices, ice spikes can form due to volume expansion, potentially damaging the device shell. This study investigates the factors influencing ice spike formation. A solid-liquid-gas numerical model with detailed thermophysical parameters, including density, specific heat capacity, thermal conductivity and viscosity, was developed to simulate ice spike formation in the energy storage chamber. The study examined the impact of cold source boundary strength, location of the cold source, initial liquid level, cavity thermal conductivity, and temperature difference on ice spike formation. Results indicate that compared with the benchmark, the larger cold source boundary strength generates a 18.23% larger incremental angle, 12.67% shorter solidification time, and 8.48% higher ice spike. The cold source is positioned at an angle between the heat conduction direction and gravitational acceleration direction. When the angle is 0°, the increment angle is the smallest, the solidification time is the shortest, and the ice spike height is the lowest. The higher ini-tial liquid level leads to a 19.43% smaller incremental angle, 4.47% longer solidification time, and 18.04% higher ice spike. Greater thermal conductivity of the cavity reduces 7.27% solidification time, while having minimal impact on ice incremental angle and height. The larger temperature difference generates a 7.73% larger incremental angle, 32.82% shorter solidification time, and 20.21% higher ice spike.

Key words: *phase change energy storage, phase interface, ice spike height, ice incremental angle, solidification time*

1. Introduction

With the rapid development of industry, energy storage and management has become an important research field. Over the past few decades, researchers have delved into energy storage technology to enhance energy distribution across different time frames and geographical locations [1,2]. The widespread implementation of large-scale solar thermal power generation has spurred the advancement of phase change energy storage (PCES) technology [3]. PCES technology not only enhances energy efficiency but also serves as a tool for temperature regulation [4,5]. In aerospace, PCES technology is frequently utilized to regulate the system temperature of artificial satellites [6,7].

The thermal control system of a spacecraft plays a crucial role in ensuring the spacecraft's stability and safety. As the spacecraft orbits, it experiences a significant increase in radiation when passing through its perihelion and a rapid decrease when passing through its apogee [8]. Therefore, it is imperative to provide a reliable and durable thermal control system for the spacecraft. In situations where the spacecraft passes through its perihelion or utilizes high-power equipment, the primary radiation radiator may struggle to dissipate the total heat load [9].

The solid-liquid PCES device can absorb excess heat from the thermal control system by undergoing phase change, and release heat by repeating the phase change process during periods of low heat load. Latent heat thermal energy storage maintains a nearly constant temperature during the heat energy storage process, storing energy by altering the phase state [10]. Talebzadegan et al. [11] found that with the decrease of Carreau index and porosity, the melting time of non-Newtonian phase change materials is shortened. While with the increase of Rayleigh number, Stefan number and Darcy number, the melting time decreases. Zhang et al. [12] found that under the same temperature change, compared with ordinary gypsum, phase change energy storage gypsum can effectively slow down the indoor temperature fluctuation and improve the living comfort. Xie et al. [13] found that heat storage tanks equipped with phase change energy storage devices have higher discharge temperature and better operating efficiency than conventional tanks without phase change heat storage devices.When the required phase change temperature is close to 0 °C, water is a suitable phase change material (PCM). Water-ice phase change offers higher latent heat, thermal conductivity, and density compared to paraffin. Experimental results show that the overall mass of equipment using water-ice phase change is approximately 70% lower than that of paraffin phase change with the same heat storage capacity [14]. However, the volume expansion of water-ice phase change is severe and inevitable, which will cause substantial mechanical pressure on the package shell of the energy storage device. Blaney et al. [15] found that the internal pressure caused by the volume expansion of the phase change material and the heat stress caused by the uneven temperature. Smykowski et al. [16] found that the location of potential damage depends on whether the stresses come from the temperature gradient in the material of the tube or from the expansion of the phase-change material. Riahi et al. [17] found that compared to an oscillating axial stress between 100 and 135 MPa and therefore exacerbated creep damage in a vertical system, tubes in a horizontal system experience a flat moderate radial stress around 100 MPa where the tube sheets can be readily designed to overcome the increase in stress. Cui et al. [18] found that in the area close to the tube wall of the heat exchange tube, the smaller the fin spacing, the thinner the thickness, the faster the phase change heat storage speed. In the central area of the PCM, the larger the fin spacing and thickness, the better the effect of phase transformation heat.

The enhanced heat transfer methods have obvious effect on improving the energy storage performance of phase change energy storage devices. Kondakrindi et al. [19] found that adding MgO nanoparticles to water as heat transfer fluid can significantly reduce the melting time. Abhinand et al. [20] found that exterior cooling with fin assistance is the case with highest cooling efficiency with least solidification time. Li et al. [21] found that compared with the phase change thermal management system without fins, the use of fractal fins can reduce the front plate temperature and improve its temperature uniformity during operation time. Ajarostaghi et al. [22] found that employing the proposed ice-on-coil ice storage equipped with a coil tube and suitable water/EG-refrigerant heat exchanger as evaporator leads to a uniform ice production around the coil. Cavieres-Garrido et al. [23] found that TiO_2 nanoparticles mainly affect the natural convection between the ice layer and the liquid phase of

the PCM by increasing the convective heat transfer coefficient. Zhang et al. [24] found that the strengthening effect of metal fins on the solidification process of paraffin wax is better than that of nano metal oxide particles. Chandrasekaran et al. [25] found that the addition of iron oxide nanoparticles to deionized water significantly improved the uniformity of heat flux density in the container within the first 25% of the entire solidification process. Wang et al. [26] found that under appropriate rib spacing, slender ribs can enhance the synergistic effect of paraffin temperature field and flow field changes, and increase the heat transfer rate. Li et al. [27] found that with the increase of fin width, thickness, height and number of circumferential fins, the heat storage and release time of the heat exchange tube decreases.

In addition, the researchers improved the energy storage performance in the phase change device by using active enhanced heat transfer technology. Larki et al. [28] found that the vortex generators system can increase the turbulence intensity in the center of the tube, reduce the flow boundary layer, and enhance the thermal boundary layer. Therefore, the heat transfer efficiency of the phase change heat storage is effectively improved. Huang et al. [29] found that adding rotating machinery to the triple-tube energy storage system can improve the heat transfer uniformity inside the device.

There are few studies on the effect of water-ice phase change volume expansion on the energy storage cavity in the literature. Some studies in the aerospace field indicate that the main challenge in using WPCES devices is the potential for leakage accidents due to volume expansion during the water solidification process. Hansen et al. [30] studied water-based phase change devices structural damage and failure with plate and microtube packaging. The place where the structure of the WPCES device is damaged may be where the water is finally solidified, and more voids need to be arranged in this area. Hansen et al. [31] continued to optimize the micro-tube heat exchanger. However, the volume expansion still causes the microtubules to bend and leak. Leimkuehler et al. [32] designed various void structures to control water's solidification process to meet the volume expansion of water. Finally, the energy storage device did not suffer severe structural damage after 90 thermal cycles. Lee et al. [33] integrated the WPCES device with the radiation radiator based on the vacuum environment and actual lunar surface temperature. However, there was a certain degree of leakage in both experimental devices. Zhang et al. [34] found that under the condition of constant satellite power, the plate phase change energy storage heat exchanger composed of 20 layers of PCM, 17 layers of internal fluid circuit and 2 layers of external fluid circuit has good heat dissipation capacity for special payloads with high power and short-term periodic working characteristics.

For microgravity environment in spacecraft, PCM leakage caused by ice spike is is not conducive to the work of the system. In addition, the thermal environment during the operation of the spacecraft is complex. The use of equipment is limited by the structure and operation direction of the spacecraft. Therefore, in order to investigate a high quality water based phase change device, it is necessary to study the mechanism of ice spike. While the current research focuses on how to improve the energy storage performance of the phase change device, and lacks the safety research of the packaging structure. Therefore, it is urgent to study the influence mechanism of key factors in practical application on ice peak formation.

On the basis of the previous research, this paper studies the ice spike formation of water-based phase change energy storage device. The WPCES device is simplified into a rectangular cavity. Considering the serious volume expansion of water-ice phase change, appropriate space is reserved in the energy storage device. And a solid-liquid-gas numerical heat transfer model is established. The for-

mation of ice spike in the device is simulated by combining the VOF model and the solidification/melting model. The mesh adaptive method is applied to accurately capture the phase interface. The key factors of ice spike formation, including cold source boundary strength, cold source position, initial liquid level, square cavity thermal conductivity and temperature difference, are studied by comparing with typical working conditions.

2. Numerical modeling

2.1. Physical model

The WPCES device is simplified as a copper square cavity. Fig. 1 shows the geometric model of the square cavity. Due to the symmetric, only 1/2 domain of the cavity is simulated. For the convenience of analysis, this paper also made the following assumptions: 1) Liquid water and air flow are laminar flow, 2) Neglecting viscous dissipation, 3) Neglecting heat dissipation.

Case P1 aligns with most scenarios encountered in practical applications. Hence, this study scrutinizes various cases relative to case P1 to delve deeper into the critical factors influencing ice spike formation. The volume expansion of water-ice phase change is about 10%, so enough space needs to be reserved inside the energy storage device to adapt to the volume expansion of water-ice phase change. In addition, the structure of the energy storage device will affect the phase change process. Therefore, it is necessary to consider the specific relationship between the filling ratio of water and the cavity structure. The geometric dimensions of P1 are detailed below. The cavity wall thickness measures 1 mm. The initial water volume fraction, η (defined as the ratio of h to H), is set at 80%. S, representing the area of water (the product of L and h), equals 1600 mm². The inner width, L, is 50 mm, while the inner height, H, measures 40 mm. The water height, h, is 32 mm. Gravitational acceleration, g, is -9.81 m·s^{-2}. The aspect ratio of water, r (h/L), is 0.64. The thermal boundary condition is that the outer surface of bottom wall maintains a constant temperature of 253.15 K, and the upper and side walls are insulated. Initially, the temperature of the cavity and the water it contains is 283.15 K.

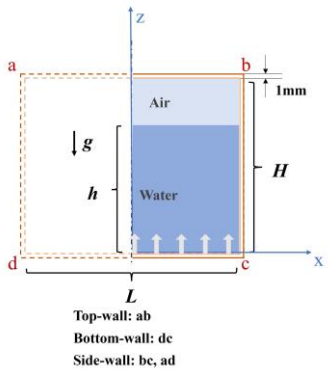

Fig. 1. Geometrical configuration of the physical model

Based on case P1, the phase interface characteristics were described in the early stage by incremental angle and ice spike height. And according to the increment angle, five key moments are selected(τ_0~τ_4), and the ice spike formation process is divided into four stages: the sidewall cooling effect stage, the thin ice layer stage, the upper wall cooling effect stage and the ice spike stage [35]. The angle between the solid-liquid interface and the horizontal line is the incremental angle. And the average incremental angle $\overline{\theta}$:

$$\bar{\theta} = \int_0^{\frac{L}{2}} \frac{\theta(x)}{L/2} dx \tag{1}$$

The ice spike height (h_p) is the height difference between the ice peak and the initial water level. The slope of solid-liquid interface k_s is calculated by the coordinate, shown in Eq. (2), and the anti-trigonometric function of k_s calculates the incremental angle θ.

$$k_s = -\frac{z_{n+1} - z_n}{x_{n+1} - x_n} \tag{2}$$

2.2. Numerical method

When the VOF model is applied to the multiphase flow problem, the control equations of each phase are shared, and they are linked by the phase volume fraction α_n. In this paper, the solution region includes two phases: the first phase is air, and the air volume fraction in the unit is α_1; the second phase is liquid water, and the volume fraction of water in the unit is α_2. When $\alpha_2 = 0$, the unit is filled with air; when $0 < \alpha_2 < 1$, the liquid water and air coexist in the unit; when $\alpha_2 = 1$, the unit is filled with liquid water. The solidification/melting model is an important method to study the solid-liquid phase transition. The solidification/melting module embedded in the commercial software FLUENT is used to calculate the solidification/melting process. The model introduces a variable liquid fraction β, which can represent the phase state of the phase change material. When the liquid fraction β of a unit is 1, it means that the phase change material of this unit is all liquid. When the liquid fraction β of a unit is 0, it means that the phase change material of this unit is all solid. When the liquid fraction β of a unit is between 0 and 1, the solid and liquid phase change materials of this unit coexist. Based on the above settings, the control equation are as follows :

Continuity equation:

$$\frac{\partial \rho \alpha_n}{\partial \tau} + u_i \frac{\partial \rho \alpha_n}{\partial x_i} = 0 \tag{3}$$

Momentum equation:

$$\frac{\partial}{\partial \tau}(\rho u_i) + \frac{\partial}{\partial x_j}\left(\rho u_i u_j\right) = -\frac{\partial P}{\partial x_i} + \frac{\partial}{\partial x_j}\left(\mu \frac{\partial u_i}{\partial x_j} + \mu \frac{\partial u_j}{\partial x_i}\right) + \rho g_i + S_i \tag{4}$$

Energy equation:

$$\frac{\partial}{\partial \tau}(\rho u_i) + \frac{\partial}{\partial \tau}\rho E + u_i \frac{\partial}{\partial x_i}(\rho u_i E) = \frac{\partial}{\partial x_i}\left(k \frac{\partial T}{\partial x_i}\right) \tag{5}$$

where ρ is the density, τ is the time, u_i is the velocity component, and x_i is the Cartesian coordinate. g is the gravitational acceleration. And P, μ, k are pressure, dynamic viscosity, thermal conductivity respectively. S_i is source term [36].

$$S_i = -A \frac{(1-\beta)^2}{\beta^2 + \varepsilon} u_i \tag{6}$$

where ε is a small value,which equals 0.001. ε can avoid floating-point overflow in the calculation process. A is called the mushy zone constant, which affects the shape of the mushy region. A is crucial to the solidification and melting rate. Zeneli et al. [37] suggested that $A = 5\times10^5$ is more accurate for simulating the melting process, and the larger value $A = 10^6$~10^9 is recommended for the simulation of

the solidification process. Dallaire et al. [38] used the value of $A = 10^7$ to study the natural convection of water solidification process, and this method and numerical value are also used in this study. β is the liquid fraction:

$$\beta = \begin{cases} 0 & T < T_S \\ \dfrac{T - T_S}{T_l - T_S} & T_S < T < T_l \\ 1 & T_S < T \end{cases} \tag{7}$$

where T is the average temperature of water, T_s is the solidification temperature and T_l is the melting temperature.

E is the specific enthalpy:

$$E = H_l + E_s \tag{8}$$

where H_l is the latent heat and E_s is the sensible enthalpy.

The sensible enthalpy:

$$E_s = E_{ref} + \int_{T_{rof}}^{T} c_p dT \tag{9}$$

where E_{ref} is the reference sensible enthalpy. c_p is the specific heat.

The latent heat:

$$H_l = \beta H_{water} \tag{10}$$

where H_{water} is the latent heat of water.

The thermophysical parameters of water and air, such as density, specific heat capacity, thermal conductivity and viscosity, are fitted by Peng-Robinson equation [35].

2.3. Grid independence verification and model validation

In this study, the transient numerical simulation of the model is carried out by VOF and solidification/melting model. The PISO algorithm is utilized to manage the pressure-velocity coupling scheme. For the spatial discretization of pressure, the “PRESTO!” method is applied. The spatial discretization of density and momentum is achieved using the "Second Order Upwind" method. For the discretization scheme of energy and volume fraction, the "Geo-Reconstruct" and "Quick" methods are employed, respectively. The convergence criteria are set to 10^{-9} for continuity, velocity and energy. And the time-step is established at 0.002 s. The calculation accuracy is set to double precision. And the mesh adaptive method is used to capture the accurate phase interface.

It is found that the number of grid has less effect on the liquid fraction of water. The independence of the grid is confirmed by P1 using three different grid sizes of 0.1 mm, 0.2 mm, 0.4 mm, with grid components numbering 108262, 26832, and 6592, respectively. Figure 2 displays the liquid fraction as time progresses. And it is important to highlight that the grid size has minimal impact on the liquid fraction. The mass average liquid phase fraction in Fig. 2 also shows that the calculation model applying the grid adaptation method is still grid-independent.

In past research conducted by the study team, experiment confirmed the dependability of the numerical approach [35]. The experimental system consists of six sub-systems. (1) The incubator

LRH-150/250F is used to provide the initial temperature with 283.15 K for the test cavity, and the temperature separation is ± 0.1 °C. (2) The test cavity is made of copper, and it is a hollow cube with a height of 50 mm and a width of 50 mm; other sizes are the same as Case P1. The side-wall and top-wall are covered by insulation cotton with 25 mm thickness. (3) The cryostat DC-3015 is used to provide the cooling capacity for the coolant; the temperature fluctuation is ± 0.05 °C. (4) The coolant in the tank is glycol solution. The coolant can provide a cold boundary of 253.15 K for the ektexine of bottom-wall. (5) The temperature detector DT-1311 collects data from a thermocouple, and the accuracy is ± 0.1 °C. (6) The photography system is used to record the moving interface. The power of the optical positioner is 30 mW, and the diameter of the micro-camera is 3.9 mm.

The geometric size of the numerical model used for verification is consistent with the experimental square cavity. And boundary conditions are the same as those of P1. Illustrated in Fig. 3, the characteristics observed in experiment of the interface align with those of the numerical model. The final numerical liquid level is 39.4 mm, 8.58% lower than the experimental liquid level (43.1 mm). This slight difference may be caused by two aspects. Firstly, air bubbles result in a larger volume expansion and a higher height of experimental ice spike. Secondly, the tilt of the optical positioner and micro-camera result in inaccurate height of air interface. In conclusion, the numerical model is deemed trustworthy for simulating the solidification process of water within cavities.

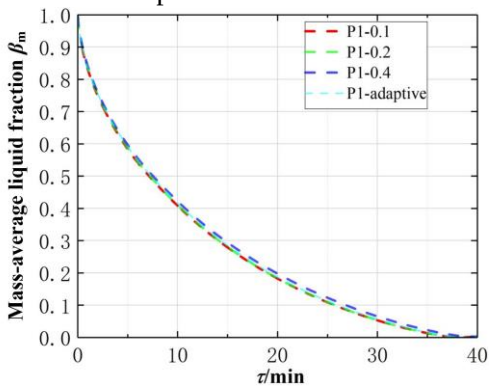

Fig. 2. Mass-average liquid fraction with three kinds of grids

(a) The experimental system[35]

(b) Ice spike in the test cavity[35]

Fig. 3. Diagram of the experimental system

3. Results and discussion

3.1. Effect of cold source boundary strength on ice spike characteristics

The cold source boundary of P1 is the bottom wall, and the temperature of the bottom wall is 253.15 K. The cold source boundary of P0 is the bottom wall, and the temperature of the bottom wall is 253.15 K, but the side and top walls of P0 are adiabatic. The cold source boundary of P2 is the bot-

tom and the side walls, and the temperature of the bottom and the side walls is 253.15 K. By comparing cases P0 and P1, the indirect heat transfer effect of the sidewall is investigated. By comparing cases P0 and P2, the direct heat transfer effect of the side wall is analyzed.

Fig. 4 shows the influence of the boundary strength of the cold source on the incremental angle. In order to analyze P0, the key time of P0 is calculated based on the dimensionless time ($\Gamma = \tau/\tau_4$) of P1 at each critical time. Tab. 1 shows that the incremental angle of P0 is always zero because P0 does not form an ice spike. The average increment angle of P2 is 18.23% larger than P1. The reason is that the cold source temperature of the P2 is constant, and the cooling effect is more substantial under the direct heat transfer.

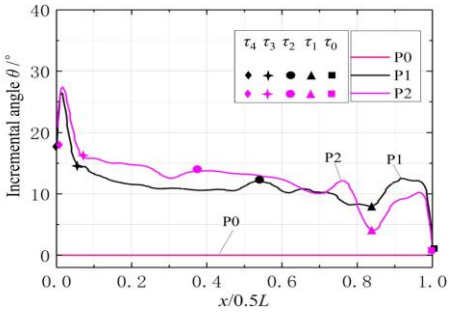

Fig. 4. The effect of boundary strength of cold source on the increment angle

Tab. 1. Average increment angle, solidification time and ice spike height under different boundary strength of cold source

Case	$\overline{\theta}$/°	Deviation	τ_4/min	Deviation	h_p/mm	Deviation
P1	10.86	—	37.96	—	4.60	—
P0	0	—	70.48	+85.66%	0	—
P2	12.84	+18.23%	33.15	-12.67%	4.99	+ 8.48%

Fig. 5(a) is the interface of P0. The dashed line is the water-air interface, and the real line is the solid-liquid interface. The reason is that the side wall of P0 is adiabatic, therefore, P0 is a one-dimensional heat conduction model, and its interface moves up uniformly. Fig. 5(b) is the interface of P2. There is little difference between the characteristics of each stage of the ice spike formation process of P2 and P1.

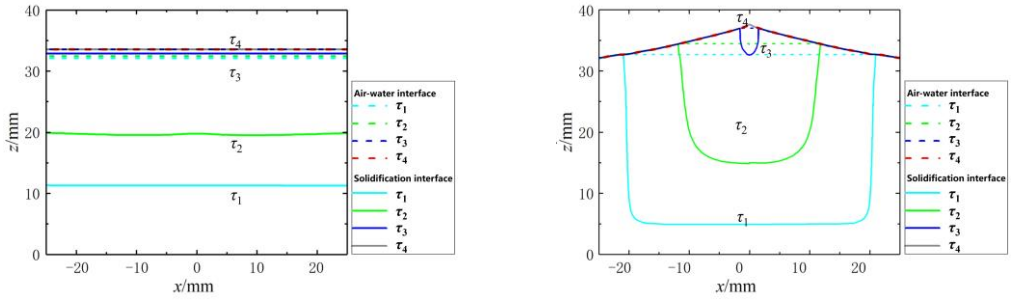

(a) Phase interface of example P0 (b) Phase interface of example P2

Fig. 5. The effect of boundary strength of cold source on the phase interface

The solidification time of P0 is 85.66 % longer than P1. The reason is that the thickness of solid ice increases over time, the thermal resistance of solid ice increases with time. Therefore, the later solid-ification process becomes slow. The solidification time of P6 is only 12.67 % shorter than P1. The reason is that due to the favorable thermal conductivity of the side wall material copper, the actual cold source boundary of P6 and P1 is similar. This means that heat can be transmitted through the side

wall, thereby enhancing heat transfer. Therefore, the greater the cold source boundary strength, the shorter the solidification time.

In summary, the side wall of the copper square cavity has an indirect heat transfer effect. The stronger the cold source boundary strength is, the larger the increment angle is, and the higher the ice spike height is. The greater the boundary strength of the cold source, the shorter the solidification time.

3.2. Influence of Cold Source Location on Ice Spike Characteristics

Fig. 6 shows the angle ω between the direction of heat conduction and gravity acceleration, which characterizes the location of the cold source. The cold source of P1 is the bottom wall. During the solidification process, the liquid water transfers heat to the bottom wall, and the direction of the heat conduction is downward, the same as gravity acceleration, and ω=0°. Case P1 conforms to the application of ground static energy storage equipment. Cases P3 (ω=90°) and P4 (ω=180°) conform to the application of aerospace or ground motion energy storage equipment. The example P3 is an asymmetric thermal boundary, so all the computational domains are simulated.

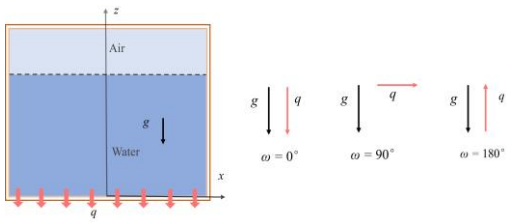

Fig. 6. The angle ω between the direction of heat conduction and gravity acceleration

Fig. 7 shows the influence of location on the increment angle θ. Tab. 2 shows the average incremental angle, solidification time and ice spike height under different gravity acceleration directions. P3 is asymmetric about the z-axis, so the increment angle is the angle in the full coordinate range. The increment angle is positive in the range of $x/0.5L$ =-0.14~1. In $x/0.5L$=-1~-0.14, the incremental angle is negative. This is because the liquid water of P3 is only cooled by the right wall, and the liquid water on the right side solidifies faster than the left, so the average increment angle on the left side is larger.

The mean incremental angle for P4 is 14.38°. The first stage shows only a minor increase in angle, whereas the subsequent second, third, and fourth stages exhibit a progressively larger incremental angle. This phenomenon occurs because P4's cold source is located at the upper wall. Due to the delayed response in wall heat transfer, the temperature of the sidewall does not decrease quickly during the initial stage, resulting in a less pronounced cooling effect of the sidewall at this stage.

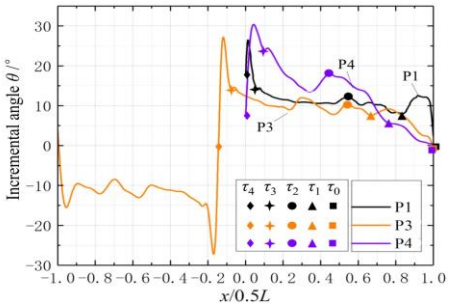

Fig. 7. The influence of gravity acceleration direction on the incremental angle

Tab. 2. The average increment angle, solidification time and ice spike height under different cold source locations

Case	ω/°	$\overline{\theta}$/°	deviation	τ_4/min	deviation	h_p/mm	deviation
P1	0	10.86	—	37.96	—	4.60	—
P3	90	10.76 -12.31	-0.92% +13.35%	44.66	+17.65%	5.08	+10.43%
P4	180	14.38	+32.41%	48.33	+27.31%	6.26	+36.09%

Fig. 8(a) is the phase interface of case P3. The characteristics of each stage of case P3 significantly differ from those of P1. The solidification and air interfaces of each stage of P3 are asymmetric about the *z*-axis. The reason is that the cold source of case P3 is the right wall, and the right wall transmits the cold energy to the left wall through the upper wall and the bottom wall. Therefore, the cooling near the left wall lags and the formed interface is asymmetric.

Fig. 8(b) is the interface of case P4. The characteristics of each stage of case P4 also differ from P1. The 'u-shaped' solidification interface of case P4 is small upper and large lower. The reason is that the cold source is on the upper wall, and transmits the cold energy to the bottom of the device through the side wall. Hence, the area near the side wall cooled faster than the bottom wall. And the ice spike height of P3 is 10.43 % higher than P1, and the ice spike height of P4 is 36.09 % higher than P1. This is because the greater the angle between the direction of heat flux density and acceleration of gravity, the smaller the incremental angle in the initial stage and the larger in the later stage.

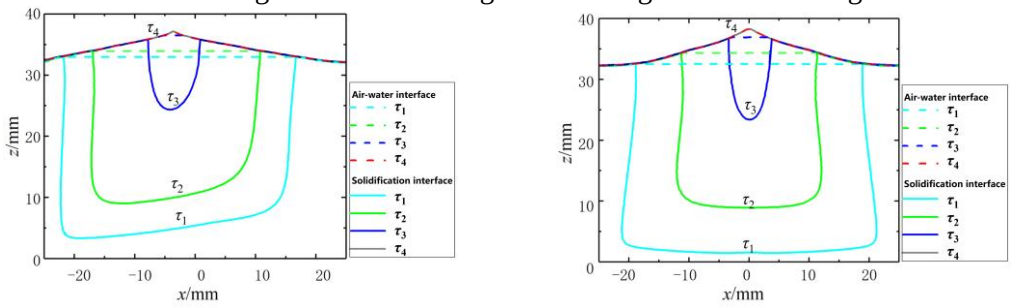

(a) Case P3 (b) Case P4

Fig. 8. The effect of gravity acceleration direction on the phase interface

The solidification time of P3 is only 17.65% longer than P1. And the solidification time of P4 is 27.31% longer than P1. The reason is that the smaller the direction angle is, the more direct the heat conduction between the cold source and liquid water is.

3.3. Effect of Initial Liquid Level on Ice Spike Characteristics

Tab. 3 shows cases of different initial liquid levels. The upper walls of P1, P5 and P6 are sealed, and the upper wall of P7 is not sealed. Analyzing cases P1, P5 and P6, the influence of liquid level height on ice spike is analyzed. Comparing cases P5 and P7 permits an analysis of the influence of the upper wall on ice spike characteristics.

Tab. 3. Cases of different initial liquid level conditions

Case	*h*/mm	η	The package of upper wall
P1	32	0.8	encapsulation
P5	35	0.875	encapsulation
P6	29	0.725	encapsulation
P7	35	0.875	not-encapsulating

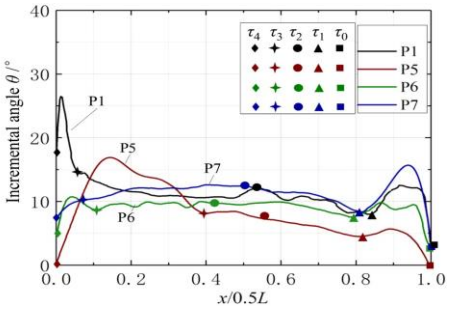

Fig. 9. The influence of initial liquid level on incremental angle

Fig. 9 shows the effect of the initial liquid level on the increment angle. Tab. 4 shows the average increment angle, solidification time and ice spike height under different initial liquid levels. The fourth stage of P5 is longer, and the incremental angle finally reduced to 0°. The reason is that the initial liquid level of case P5 is too high, and the air interface in the fourth stage is too close to the upper wall. The rapid solidification of the three-phase thin ice layer limits the upward movement of the air interface and the formation of small ice spike.

Tab. 4. Average increment angle, freezing time and ice spike height at different initial liquid levels

Case	h/mm	The package of upper wall	$\overline{\theta}$/°	deviation	τ_4/min	deviation	h_p/mm	deviation
P1	32	encapsulation	10.86	—	37.96	—	4.60	—
P5	35	encapsulation	8.75	-19.43%	39.66	+4.47%	5.43	+18.04%
P6	29	encapsulation	9.17	-15.56%	34.08	-10.22%	4.45	-3.16%
P7	35	not-encapsulating	11.17	+2.85%	42.83	+27.31%	5.33	+15.87%

The average incremental angle of P6 is 15.56% smaller than P1 due to the liquid water level of the case P6 is low, resulting in less longitudinal expansion. The average incremental angle of case P7 is 27.65% larger than case P5. The reason is that the case P7 has no upper wall and no thin ice layer constraint, which make its increment angle larger.

Fig. 10(a) is the interface of case P5. The air interface of case P5 is relatively smooth. The reason is that the upper wall of case P5 increases the solid phase percentage in the three-phase thin ice layer, limiting the formation of ice spike.

Fig. 10(b) is the interface of case P6. The ice spike of case P6 is relatively flat. The reason is that the reserved air domain of case P6 is larger, and the air interface is less affected by walls and air flow.

Fig. 10(c) is the interface of case P7. Case P7 forms a small ice spike. The reason is that case P7 has no upper wall constraint, and the flow velocity of the air domain caused by the external air inflow is large, which hinders the protrusion of the small ice spike. Secondly, case P7 does not form a thin ice layer, which further proves that the upper wall cooling effect is the root cause of the thin ice layer.

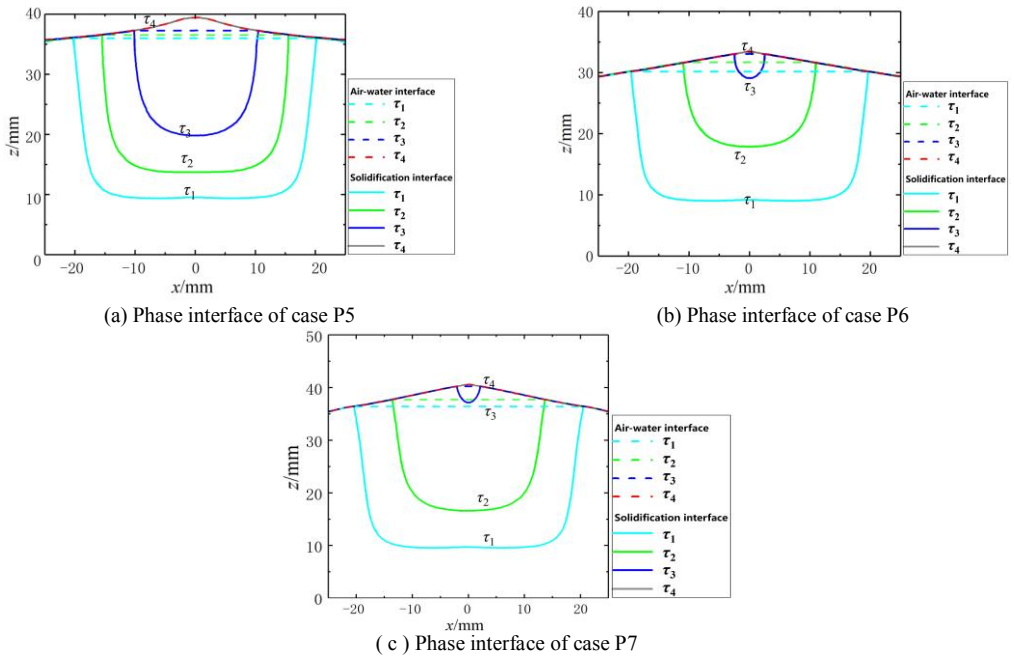

(a) Phase interface of case P5

(b) Phase interface of case P6

(c) Phase interface of case P7

Fig. 10 The effect of initial liquid level on the phase interface

Case P5 has a solidification time that is 4.47% lengthier compared to Case P1, while Case P6 experiences a 10.22% reduction in solidification time when compared to Case P1. This disparity occurs due to the direct correlation between the initial liquid level and the amount of liquid water to be solidified, resulting in an extended solidification time. Furthermore, Case P7 shows a 7.99% increase in solidification time relative to Case P5, which can be attributed to the absence of a sealed upper wall causing a significant dissipation of cold energy from the storage cavity.

3.4. Effect of Cavity Thermal Conductivity on Ice Spike Characteristics

The cavity material of case P1 is copper, the thermal conductivity is 387.6 $W \cdot m^{-1} \cdot K^{-1}$, and the cavity thickness is 1 mm. The thickness of case P8 is 3 mm. The material of case P9 is aluminum alloy 6061T6, the thermal conductivity is 167 $W \cdot m^{-1} \cdot K^{-1}$. And the other boundary conditions of P8 and P9 are the same as case P1. By comparing cases P8 and P1, the influence of thickness on ice spike characteristics is analyzed. By comparing cases P9 and P1, the influence of the thermal conductivity on the ice spike is analyzed.

Fig. 11 shows the effect of thermal conductivity on the increment angle. The characteristics of the three incremental angle curves are the same. Tab. 5 shows the average increment angle, solidification time and ice spike height under different thermal conductivity. The average increment angles of case P8 and case P9 are similar with P1. Fig. 12 shows that the phase interface characteristics of the cases P8, P9 and P1 are slightly different.Therefore, the thermal conductivity of the cavity has little effect on the incremental angle.

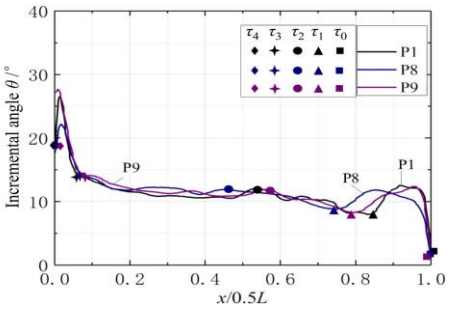

Fig. 11. Effect of thermal conductivity on increment angle

Tab. 5. Average increment angle, solidification time and ice spike height under different cavity thermal conductivity.

Case	$\overline{\theta}$/°	deviation	τ_4/min	deviation	h_p/mm	deviation
P1	10.86	—	37.96	—	4.60	—
P8	11.81	+8.75%	35.20	-7.27%	4.62	+0.43%
P9	11.86	+9.21%	37.10	-2.27%	4.71	+2.39%

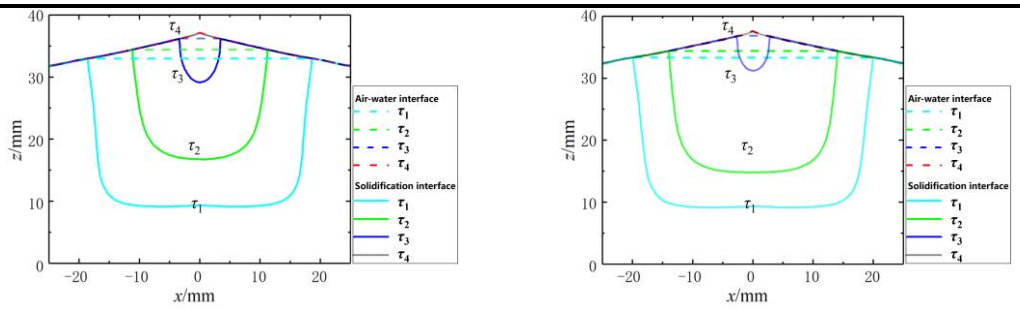

(a) Phase interface of case P8 (b) Phase interface of case P9

Fig. 12. Effect of thermal conductivity of square cavity on phase interface

P8's solidification time is just 7.27% less than P1's, while P9's solidification time is only 2.27% shorter than that of P1. Thus, the thermal conductivity of the square cavity has minimal impact on both the liquid phase fraction and solidification time.

3.5. Effect of Temperature Difference on Ice Spike Characteristics

Taking the satellite orbiting the earth as the background, the bottom wall temperature of case P1 is 253.15K, and the initial temperature of liquid water is 283.15K. The bottom wall temperature of case P10 and case P11 are 243.15K and 263.15K, respectively. And the other boundary conditions are the same as case P1. By comparing cases P1, P10 and P11, the influence of temperature difference ΔT between the bottom wall and liquid water on ice spike characteristics is analyzed.

Fig. 13 shows the effect of bottom wall temperature on the incremental angle. Tab. 6 shows the solidification characteristic parameters under different bottom wall temperatures. The average incremental angle of P10 is 7.73% larger than P1. And the average incremental angle of case P11 is 1.20% smaller than case P1. Therefore the greater the temperature difference, the greater the increment angle.

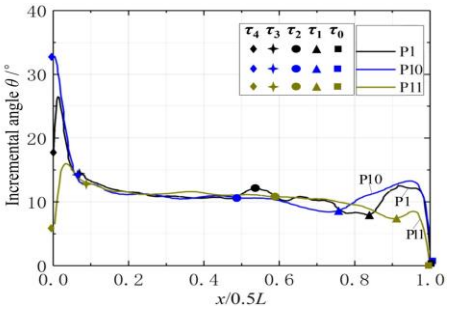

Fig. 13. Effect of bottom wall temperature on increment angle

Tab. 6. Average increment angle, freezing time and ice spike height under different bottom wall temperatures

Case	ΔT/K	$\overline{\theta}$/°	deviation	τ_4/min	deviation	h_p/mm	deviation
P1	30	10.86	—	37.96	—	4.60	—
P10	40	11.70	+7.73%	25.50	-32.82%	5.53	+20.21%
P11	20	10.73	-1.20%	72.58	+91.20%	4.31	-6.30%

Fig. 14(a) shows the phase interface of P10. Fig. 14(b) shows the phase interface of P11. The phase interface characteristics of cases P10, P11 and case P1 are almost the same, therefore, the temperature difference has little effect on the phase interface characteristics.

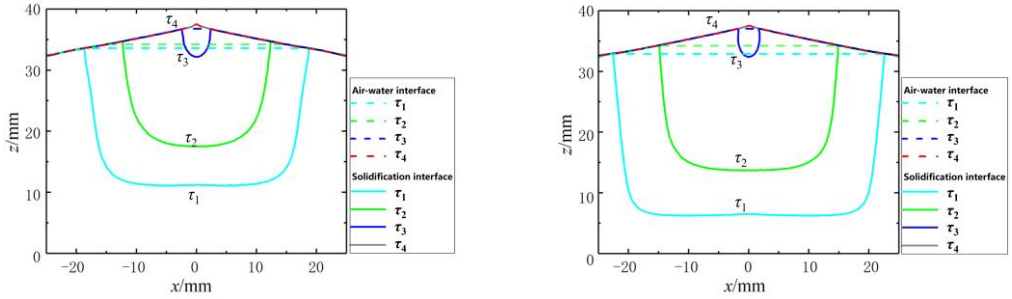

(a) Phase interface of case P10 (b) Phase interface of case P11

Fig. 14. Effect of bottom wall temperature on phase interface

The time it takes for case P10 to solidify is 32.82% less than it takes for case P1, whereas the solidification duration for case P11 is 91.20% greater compared to case P1. Consequently, a larger temperature gap results in a quicker solidification process.

4. Conclusions

This paper simplifies the water-based phase change energy storage device into a rectangular cavity to establish a phase change heat transfer model. And the effects of cold source boundary strength, cold source position, initial liquid level, cavity thermal conductivity and temperature difference on ice spike characteristics were studied.

(1) Compared with the benchmark, the larger cold source boundary strength generates a 18.23% larger incremental angle, 12.67% shorter solidification time, and 8.48% higher ice spike. The cold source is positioned at an angle between the heat conduction direction and gravitational acceleration direction. When the angle is 0°, the increment angle is the smallest, the solidification time is the shortest, and the ice spike height is the lowest. The higher initial liquid level leads to a 19.43% smaller incremental angle, 4.47% longer solidification time, and 18.04% higher ice spike. Greater thermal conductivity of the cavity reduces 7.27% solidification time, while having mini-

mal impact on incremental angle and height. The larger temperature difference generates a 7.73% larger incremental angle, 32.82% shorter solidification time, and 20.21% higher ice spike.

(2) The greater the boundary strength of the cold source, the higher the ice spike height, which is relatively dangerous. When the angle between the direction of heat conduction and gravity acceleration is 0°, the height of the ice spike is the smallest, which is beneficial to aerospace applications. The ice spike height increase with the increase of initial liquid level. The temperature difference and the thermal conductivity of the cavity have little effect on the ice spike incremental angle.

(3) The temperature difference can be given priority when safely optimizing the energy storage performance of water-based phase change energy storage device.

The application scope of this study is to provide a theoretical foundation for solving the leakage problem caused by mechanical damage and optimizing the structure of water-based phase change energy storage device. According to the key factors affecting ice spike formation, the structural sealing and energy storage performance of water-based phase change energy storage device can be selectively optimized. The limitation of this study is that this paper mainly analyzes the mechanism of ice spike formation by volume expansion when water freezes in the energy storage cavity. The theoretical results obtained from the analysis can provide a reference for the phase change materials with volume expansion at low temperature like water. However, at present, the phase change materials commonly used in practical engineering applications undergo severe volume expansion at high temperature, that is, during the melting process. Future work will focus on the study of the fluid-thermal-solid coupling between the ice spike and the square cavity walls.

Acknowledgment

This work was financially supported by the National Nature Science Foundation of China (No. 51876146).

Nomenclature

A	mushy zone constant [–]	T	temperature [K]
c_p	specific heat [J·kg^{-1}·K^{-1}]	T_l	melting temperature [K]
E	specific enthalpy [J·kg^{-1}]	T_s	solidification temperature [K]
E_{ref}	reference sensible enthalpy [J·kg^{-1}]	u	velocity [m·s^{-1}]
E_s	sensible enthalpy [J·kg^{-1}]	x	coordinate [m]
g	gravity acceleration [m·s^{-2}]		
h	water level [mm]	*Greeks*	
h_p	ice spike height [mm]	α_n	volume fraction of different phase[–]
H	inner height of cavity [mm]	β	liquid fraction [–]
H_l	latent heat [J·kg^{-1}]	η	volume fraction [–]
H_{water}	latent heat of water [J·kg^{-1}]	θ	the ice incremental angle [°]
k	thermal conductivity [W·m^{-1}·K^{-1}]	μ	dynamic viscosity [kg·m^{-1}·s^{-1}]
k_s	slop of phase interface [–]	ρ	density [kg·m^{-3}]
L	inner width of cavity [mm]	τ	time [s]
P	pressure [Pa]		
r	aspect ratio [–]	*Acronyms*	
S	sectional area [mm^2]	PCM	phase change material
S_i	source term [–]	VOF	volume of fluid
		WPCES	water-based phase change energy storage

References

[1] Roskilly,A. P., *et al*., Energy Storage Systems for a Low Carbon Future – in need of an Integrated Approach, *Applied Energy*, *137* (2015), 1, pp. 463-466

[2] Yang, T., *et al*., Seasonal Thermal Energy Storage: A Techno-Economic Literature Review, *Renewable and Sustainable Energy Reviews*, *139* (2021), 110732

[3] Bozkurt, I., The Investigation of Using Phase Change Material for Solar Pond Insulation, *Thermal Science*, *26* (2022), 2, pp. 1799-1808

[4] Steen, D., *et al*., Modeling of Thermal Storage Systems in MILP Distributed Energy Resource Models, *Applied Energy*, *137* (2015), 1, pp. 782-792

[5] Kensby, J., *et al*., Potential of Residential Buildings as Thermal Energy Storage in District Heating Systems – Results from a Pilot Test, *Applied Energy*, *137* (2015), 1, pp. 773-781

[6] Peng, H., *et al*., A Novel Thermoelectric Energy Harvester Using Gallium as Phase Change Material for Spacecraft Power Application, *Applied Energy*, *322* (2022), 119548

[7] Liu, Z., *et al*., A Review on Non-Newtonian Effects and Structure-activity Relationship of Nanoparticles Enhanced Phase Change Materials in Porous Media, *Journal of Energy Storage*, *64* (2023), 107221

[8] Choi,M, K., Using Paraffin PCM for Thermal Management of BOLAS Planetary Cubesats with Ion Thrusters, *Proceedings*, AIAA Propulsion and Energy, Florida, USA, 2019

[9] Qi, G., *et al*., Enhanced Comprehensive Performance of Polyethylene Glycol Based Phase Change Material with Hybrid Graphene Nanomaterials for Thermal Energy Storage, *Carbon*, *88* (2015), pp. 196-205

[10] Liu, Z., *et al*., Application of Phase Change Energy Storage in Buildings: Classification of Phase Change Materials and Packaging Methods, *Thermal Science*, *26* (2022), 5, pp. 4315-4332

[11] Talebzadegan, M., *et al*., Melting Process Modeling of Carreau non-Newtonian Phase Change Material in Dual Porous Vertical Concentric Cylinders, *Thermal Science*, *25* (2021), 6, pp. 4283-4293

[12] Zhang, Y., *et al*., Preparation and Characterization of Phase Change Energy Storage Gypsum, *Thermal Science*, *25* (2021), 6, pp. 4737-4748

[13] Xie, X., *et al*., Design and Performance Analysis of a Heat Pump System for Motor Phase Change Thermal Storage, *Thermal Science*, *28* (2024), 2, pp. 1229-1235

[14] Leimkuehler,T. O., *et al*., Testing and Failure Mechanisms of Ice Phase Change Material Heat Exchangers, *Proceedings*, 40th International Conference on Environmental Systems, Washington DC, USA, 2010

[15] Blaney,J. J., *et al*., Containment Capsule Stresses for Encapsulated Phase Change Materials, *Applied Thermal Engineering*, *50* (2013), 1, pp.555-561

[16] Smykowski, D., *et al*., Numerical Modelling of Thermal and Mechanical Properties of Construction Elements in a Heat Storage Unit with Phase Change, *Proceedings*, 14th International Scientific Conference: Computer Aided Engineering, Wroclaw, Poland, 2019

[17] Riahi, S., *et al*., Orientation Impact on Structural Integrity of a Shell and Tube Latent Heat Thermal Energy Storage System, *Journal of Energy Storage*, *52* (2022), 104829

[18] Cui, J., *et al*., Dynamic Numerical Study on Phase Change Thermal Storage Heat Transfer, *Thermal Science*, *25* (2021), 6, pp. 4171-4179

[19] Kondakrindi, K., *et al*., Experimental Investigation on the Influence of Nanofluids Used as Heat Transfer Fluid in Phase Change Material Based Thermal Energy Storage System, *Thermal Science*, *25* (2021), 1, pp. 643-652
[20] Abhinand, S., et al., Numerical Study of Heat Transfer Fluid Position on Solidification of PCM in Fin Assisted Thermal Energy Storage System, *Proceedings*, Advances in Fluid and Thermal Engineering: Select Proceedings of FLAME 2022. Lecture Notes in Mechanical Engineering, Noida, India, 2022
[21] Li, Q., *et al*., Numerical Investigation of Thermal Management Performances in a Solar Photovoltaic System by Using the Phase Change Material Coupled with Bifurcated Fractal Fins, *Journal of Energy Storage*, *56* (2022), 106156
[22] Mousavi Ajarostaghi,S. S., *et al*., Solidification Analysis in an Ice-on-Coil Ice Storage System: Experimental and Numerical Approaches, *Journal of Energy Storage*, *65* (2023), 107291
[23] Cavieres-Garrido, F., et al., Experimental Study of the Heat Transfer during the Ice Formation of TiO_2 Water-Nanofluid around a Helical Coil CTES System, *Applied Thermal Engineering*, *230* (2023), 120829
[24] Zhang, J., *et al*., Solidification Performance Improvement of Phase Change Materials for Latent Heat Thermal Energy Storage Using Novel Branch-Structured Fins and Nanoparticles, *Applied Energy*, *342* (2023), 121158
[25] Chandrasekaran, P., *et al*., Experimental Thermal Performance of Deionized Water and Iron Oxide Nanofluid for Cold Thermal Storage, *Environmental Science and Pollution Research*, *31* (2024), 17, pp.26330-26339
[26] Wang, N., *et al*., Heat Transfer Performance of Phase Change Energy Storage Building Materials and its Application in Energy Efficient Buildings, *Thermal Science*, *28* (2024), 2, pp.1201-1209
[27] Li, F., Application of Performance Dynamic Equation in Numerical Simulation and Optimization of Waste Heat Utilization and Storage System, *Thermal Science*, *28* (2024), 2, pp.1253-1261
[28] Larki, A. J., *et al*., Investigation of the Effects of the Detachable Vortex Generators Series on Phase Change Material Behavior in an Energy Storage System, *Journal of Building Engineering*, *52* (2022), 104384
[29] Huang, X., *et al*., Investigation and Optimization of Solidification Performance of a Triplex-Tube Latent Heat Thermal Energy Storage System by Rotational Mechanism, *Applied Energy*, *331* (2023), 120435
[30] Hansen,S. W., *et al*., Water Based Phase Change Material Heat Exchanger Development, *Proceedings*, 44th International Conference on Environmental Systems, Houston, USA, 2014
[31] Hansen,S. W., *et al*., Continued Water-based Phase Change Material Heat Exchanger Development, *Proceedings*, 45th International Conference on Environmental Systems, Houston, USA, 2015
[32] Leimkuehler,T. O., *et al*., Development, Testing, and Failure Mechanisms of a Replicative Ice Phase Change Material Heat Exchanger, *Proceedings*, 40th International Conference on Environmental Systems, Bucharest, Romania, 2010
[33] Lee, S., *et al*., Thermal Vacuum Test of Ice as a Phase Change Material Integrated with a Radiator, *Proceedings*, 43th International Conference on Environmental Systems, Houston, USA, 2013
[34] Zhang, J-M., *et al*., Flow and Heat Transfer Performance of Plate Phase Change Energy Storage Heat Exchanger, *Thermal Science*, *23* (2019), 3, pp. 1989-2000

[35] Wang, Y., et al., Study of Ice Spike Formation Mechanism in the Water-based Phase Change Energy Storage, *Journal of Enhanced Heat Transfer*, 30 (2023), 1, pp. 53-73
[36] Assis, E., *et al*., Numerical and Experimental Study of Melting in a Spherical Shell, *International Journal of Heat and Mass Transfer, 50* (2007), 9, pp. 1790-1804
[37] Zeneli, M., *et al*., Numerical Simulation of a Silicon-based Latent Heat Thermal Energy Storage System operating at Ultra-high Temperatures, *Applied Energy*, *242* (2019), 1, pp. 837-853
[38] Dallaire, J., *et al*., Numerical Modeling of Solid-Liquid Phase Change in a Closed 2D Cavity with Density Change, Elastic Wall and Natural Convection, *International Journal of Heat and Mass Transfer*, *114* (2017), pp. 903-914

Paper submitted: 06.07.2024
Paper revised: 08.08.2024
Paper accepted: 10.08.2024